Error Due to Two Dimensional Approximation in Heat Transfer Analysis of Welds

A method for evaluating the error between 3D and 2D temperature fields is devised

BY V. KAMALA AND J. A. GOLDAK

ABSTRACT. Approximating a 3D heat transfer analysis of a weld with a 2D cross-sectional analysis introduces errors in the computed temperatures. This paper reports a method for evaluating this error. The method consists of computing both the 3D and 2D temperature fields. The error is the difference between these two fields. It is shown that the errors in the 2D approximation can be eliminated by modifying the true power density distribution function. It was this type of modification that enabled previous investigations to obtain accurate results from the 2D analysis in spite of this approximation error.

A method for computing the modified power density distribution function is presented. It is shown that modeling the heating effect of the arc by a power density distribution function can be viewed as a formal method for decoupling the heat equation from the magneto-fluid dynamic equations of the arc and weld pool. In particular, it is shown that a unique power density distribution exists for every transient temperature field that can be computed by solving the fully coupled equations of the arc.

Introduction

Welding is a critical technology in building nuclear reactors, offshore structures, pipelines, ships and petrochemical plants. Yet it is unusual in that it is one of the last technologies to change from a craft to a science. The critical first step in creating a science base for the design and analysis of welds is to accurately compute the transient temperature field. This is necessary because the temperature has a first order effect on the microstructure, strain, stress and ultimately on the formation of defects in welds while they have at most a second order effect on the temperature field.

Rosenthal (Ref. 1) and Rykalin developed solutions to the heat equation for point and line heat sources and idealized geometries such as infinite plates. The limitations of these solutions are discussed in Ref. 2. Recently, models for nonlinear transient finite element heat transfer analysis of welds have been developed that remove most of these limitations (Refs. 3–7). However, the only significant study of errors in any of these methods was reported by Anderson (Ref. 8). He computed the temperature field for a 1D bar with the 2D Rosenthal solution. The difference between the two solutions was taken to be an estimate of the error in the 1D solution due to the 1D approximation of the 2D problem. He showed that the difference in the two far-field solutions is small unless the arc travel speed is low, the thermal diffusivity is high or the heat input is high. He argued that under similar conditions, the errors in the 2D approximation of a 3D problem would be small. However, he did not study the errors in the 2D approximation of a 3D problem.

KEY WORDS

2-D Heat Transf. An.
Error Analysis
Cross-Section Anal.
Computed Temperature
Heat Source Models
Finite Element Model
Heat Transfer Theory
Heat Equation
Power Density Distr.
Temperature Fields

This paper presents results of an analysis of the error in a 2D cross-sectional analysis due to the 2D approximation of a problem that is more accurately described as a 3D transient problem. Errors associated with sensors or actuators are not considered. The approach is to compute the 3D transient and 2D cross-sectional FEM solutions for equivalent meshes. The error is taken to be the difference between the 3D and 2D temperatures.

In addition, it is shown that by interpreting the power density distribution function (PDDF) as the residual in the heat equation in which the exact temperature is prescribed, the PDDF that generates the exact temperature distribution with the 2D approximation can be determined. This interpretation has the advantage that it can be viewed as a formal method of decoupling the heat equation from the magneto-hydrodynamic equations of the arc and weld pool.

Heat Transfer Theory

In heat transfer, we are concerned with energy and ignore stress, strain and displacement (Refs. 1–3). The temperature, T(x,y,z,t), as a function of spatial coordinates (x,y,z) and time, t, satisfies the following parabolic differential equation, the heat equation, at every point in the domain, Ω

$$\frac{\partial}{\partial x}k_x\frac{\partial T}{\partial x}+\frac{\partial}{\partial y}k_y\frac{\partial T}{\partial y}+\frac{\partial}{\partial z}k_z\frac{\partial T}{\partial z}+Q = c\frac{\partial T}{\partial t} \quad (1)$$

where
$Q(x,y,z,t)$ = source or sink rate of heat in $\Omega(W/m^3)$
c = volumetric specific heat ($J/m^3°C$)
k = thermal conductivity ($W/m°C$).

V. KAMALA is with the Vibrations Lab, BHEL, Corp. R&D, Hyderabad, India. J. A. GOLDAK is with the Dept. of Mechanical and Aeronautical Engineering, Carleton University, Ottawa, Canada.

If k or c are functions of T, Equation 1 is nonlinear. On the boundary of Ω, either the essential or natural boundary condition must be satisfied. The essential boundary condition can be defined as

$$T(x,y,z,t) = T(x,y,z,t)$$
on the boundary S_1:
i.e., $(x,y,z) \in S_1$: $t > 0$ (2)

The natural boundary condition can be defined as

$$k_n \frac{\partial T}{\partial n} + q + h(T - T_o) + \sigma \in \left(T^4 - T_o^4\right) = 0 \quad (3)$$

on the boundary S_2; *i.e.*, $(x,y,z) \in S_2$: $t > 0$.
$q(x,y,z,t)$ = a prescribed flux (W/m^3)
k_n = thermal conductivity normal to the surface (W/m C)
h = heat transfer coefficient for convection (W/m^3C)
T_o = ambient temperature for convection and/or radiation (C)
G = Stefan-Boltzmann constant $\in$ = (W/m^2C^4) = emissivity (the full amount of energy emitted per m^2 of a black body/h)

If radiation is included or if the convective heat transfer coefficient is temperature dependent this boundary condition is nonlinear. In addition, the initial condition must be specified for $(x,y,z) \in \Omega$

$$T(x,y,z,o) = T_o(x,y,z) \quad (4)$$

If the partial differential Equation 1, the boundary conditions of Equations 2 and 3, and the initial condition of Equation 4 are consistent, the problem is well posed and a unique solution exists. The FEM imposes a piece-wise polynomial approximation of the temperature field within each element

$$T(x,y,z,t) = \sum_{i=1}^{n} N_i(x,y,z)\ T_i(t) \quad (5)$$

where
n = the number of nodes
N = basis functions dependent only on the type of element and its size and shape

Decoupling the Heat Equation

Whether or not the heat equation is coupled to other equations such as the Navier-Stokes or MHD equations, the temperature field belongs to the Sobolev space, H_0^1. In simplistic terms, the energy and the flow of energy must be finite as expressed by the following equations:

$$\int_\Omega T^2 d\Omega < \infty \quad \text{and} \quad \int_\Omega \nabla T^2 d\Omega < \infty \quad (6)$$

If the temperature field belongs to H_0^1, the FEM solution to the uncoupled heat equation always exists regardless of whether the heat equation is coupled or not. More precisely, functions Q and q that generate a temperature field by the heat equation always exist. It is equally true that with any temperature field if H_0^1 is prescribed, the heat equation will generate unique functions Q and q.

Therefore, in order to decouple the heat equation, it is necessary to find the Q and q functions that generate the desired temperature field. In welding, functions Q and q represent the heating effect of the arc called heat source models. In solving the uncoupled heat equation, these functions account for heat transfer effects such as the heat transported by moving liquids and/or resistive heating, I^2R.

The main thrust of this paper is to show that the 2D approximation requires a different Q from the 3D discretization to account for the lack of diffusive heat transfer in the longitudinal direction.

Model for Welding Heat Sources

For welding situations where the effective depth of penetration is small and the bead symmetric, the Pavelic, Friedmann and Krutz models have been quite successful (Refs. 8–11). However, for high power density sources such as a laser or electron beam and most arcs, flux models ignore the digging action of the arc or beam that transports heat well below the surfaces and does not predict the correct weld nugget shape. In such cases a PDDF is preferred. These are called flux or PDDF heat source models. The following physical and mathematical interpretation of the flux and PDDF heat source models is now proposed.

Assume the exact temperature is known and prescribed in Equation 1. The applied flux boundary condition can be evaluated as a Lagrange multiplier. The PDDF can be evaluated as the residual in Equation 1. Of course, in the most important case, T(x,y,z,t) is sought and the flux and/or PDDF must be specified as data. Nevertheless, this interpretation will be shown to lead to useful results.

Kinematic models: to reduce computing costs of solving a full 3D heat equation, Equation 1 was simplified by assuming some terms were zero. The most popular assumption is that $\partial T/\partial z = 0$ where z is the longitudinal direction. This leads to a surprisingly subtle cross-sectional model. It is equivalent to a 3D steady state solution with the added constraint that $\partial T/\partial z = 0$. This paper is concerned primarily with the error introduced by this constraint. The double ellipsoidal PDDF proposed by Goldak, *et al.* (Refs. 12, 13), has achieved notable success in predicting the correct nugget shape and size using the cross-sectional model. This led to the hypothesis that the double ellipsoidal PDDF corresponded to the weld pool size and shape. Correct nugget shapes could not be predicted with flux or hemispherical heat source models with the cross-sectional kinematic model. In addition, the PDDF is computationally cheaper because it permits a coarser mesh than the flux model.

These considerations led to the interpretation of the PDDF as the residual in the heat equation when the temperature is prescribed.

Though the hemispherical heat source is expected to model an arc weld better than a disc source, it has its own limitations. The molten pool in many welds is far from spherical. Also, a hemispherical source is not appropriate for welds that are not spherically symmetric such as strip electrode, deep penetration electron beam or laser beam welds. These limitations can be overcome by using the appropriate power density distribution function such as the double ellipsoidal volume source (Ref. 3). Speed of the torch is also modeled in this. However, a hemispherical source, which is a special case of a double ellipsoidal PDDF, is used in this analysis.

Errors in the 2D Analysis

In order to estimate the error due to 2D approximation, first a 3D transient heat transfer analysis is carried out with a hemispherical heat source (Refs. 3, 4). Then a 2D heat transfer analysis is carried out for the equivalent mesh. The results of the 2D analysis are projected onto the 3D mesh and the two temperature fields are compared.

The difference is the error due to 2D approximation. In both 2D and 3D, Equation 1 was solved with the same PDDF.

The comparison can also be made in another way. First a 3D analysis was carried out in which Equation 1 is solved for temperature with the hemispherical PDDF. Then a 2D cross-sectional analysis is carried out in which the temperatures obtained from the 3D analysis are prescribed. In this 2D analysis, the temperatures are known and Equation 1 is solved for Q, the PDDF. This generates the reactions; *i.e.*, thermal loads. These are the discrete form of the PDDF for the cross-sectional analysis. The two thermal loads can be compared; *i.e.*, in the heat equation

$$\nabla \cdot k \nabla T + Q = C \frac{\partial T}{\partial t} \quad (7)$$

$\nabla \cdot k\nabla T$ & $C\frac{\partial T}{\partial t}$ are obtained from 3D analysis and Equation 7 is solved for Q. This Q will be different from the Q obtained from the hemispherical PDDF that was used in the 3D analysis. Both PDDFs produce the same temperature field. This proves any T(x,y,z,t) that satisfies Equation 1 can be computed with the cross-sectional model, given the correct PDDF.

Results and Discussion

The 3D and 2D FEM mesh used for computing the temperature field is shown in Fig. 1. The 2D mesh is a cross-section of the 3D mesh.

Test Data

The weld analyzed was an AISI 1020 carbon steel plate 1.27 cm thick. The temperature-dependent volumetric specific heat and thermal conductivity published by BISRA (Ref. 14) was used for the calculation. Due to symmetry, only one-half of a 10.16 X 10.16 X 1.27-cm (4 X 4 X 0.5-in.) bar was analyzed — Fig. 1. All the boundaries except the top surface were assumed insulated. On the top surface, the portion just under the arc was assumed insulated during the time the arc was playing upon the surface. The domain was discretized into 284, 8-noded bricks to form an FEM mesh for 3D analysis. Smaller elements were specified where the temperature gradients were expected to change most rapidly. The special grading elements used are described in Refs. 12 and 13. The arc traveled the distance of 2.54 cm at a rate of 0.508 cm/s in 41 time steps with a power of 1.785 kW. Then the source was removed and the weld allowed to cool.

The temperature contours obtained with the 3D analysis on section AA (Fig. 1) for different time intervals are given in Fig. 2. The temperature contours obtained with 2D cross-sectional analysis for the same problem (plane AA) with approximately the same PDDF at the corresponding time intervals are given in Fig. 3. The initial location of the arc from the 2D plane (AA) and the speed of the torch are taken to be the same in both cases for better comparison. This also provides a measure of the cross-sectional size of the weld metal zone (WMS) and heat affected zone (HAZ). From Figs. 2 and 3, one may observe that the maximum temperature developed at different nodes at any given time was always higher in the 3D analysis than the 2D cross-sectional analysis with the hemispherical PDDF. This confirms that the effect of temperature gradient in the longitudinal direction is signifi-

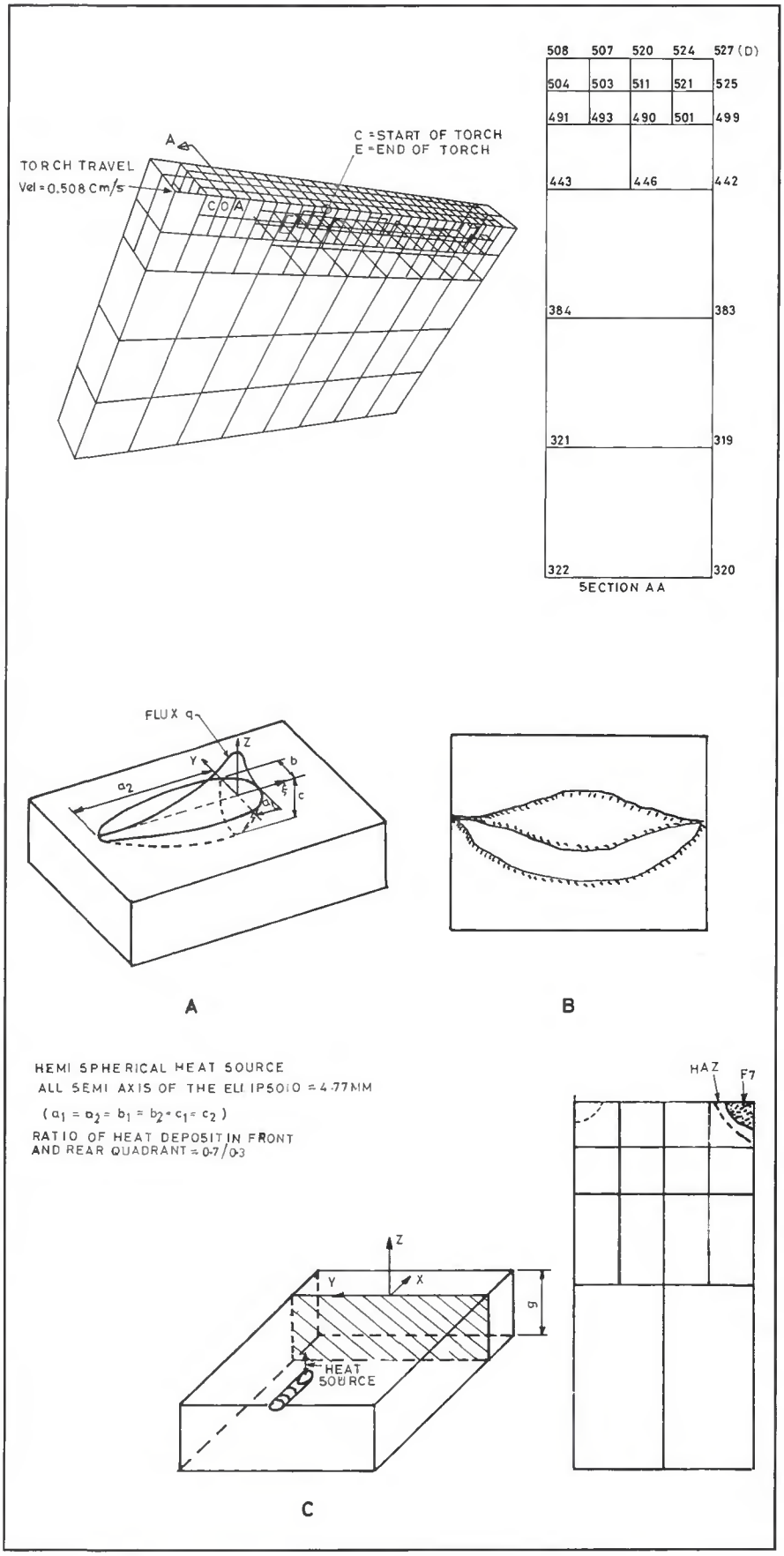

Fig. 1 — FEM mesh used for 3D and 2D analysis.

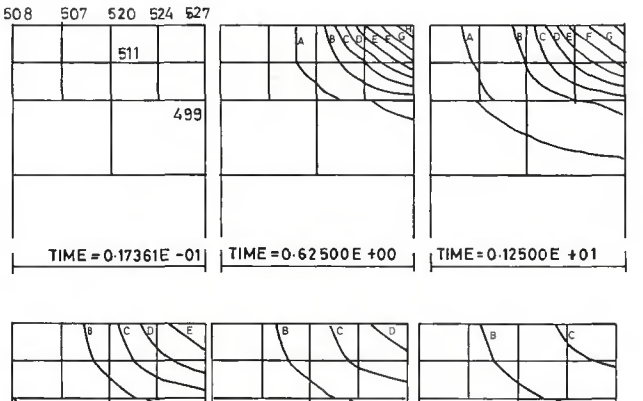

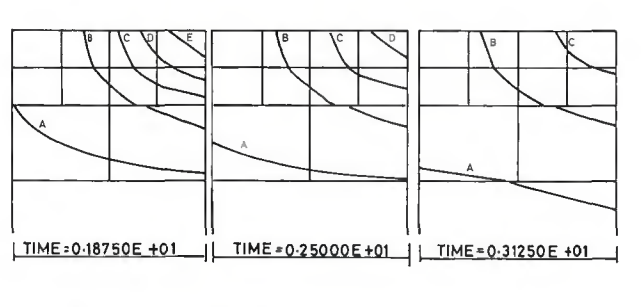

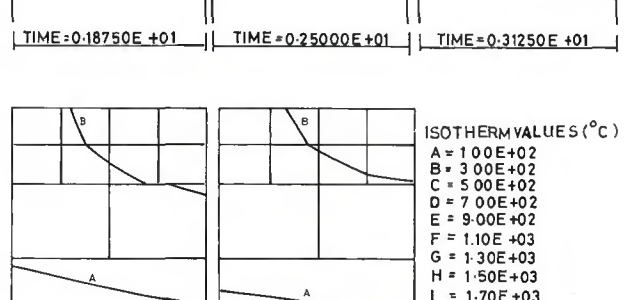

Fig. 2 — Temperature field computed using 3D analysis (section AA).

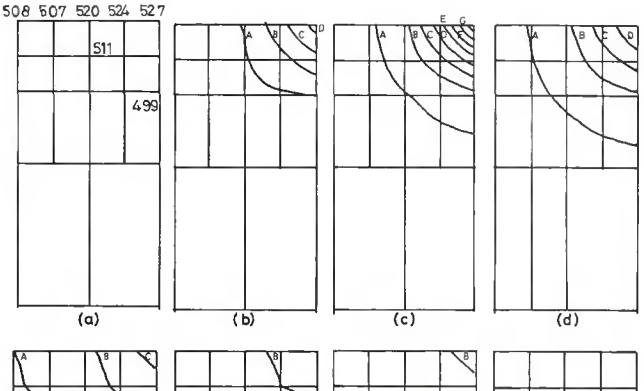

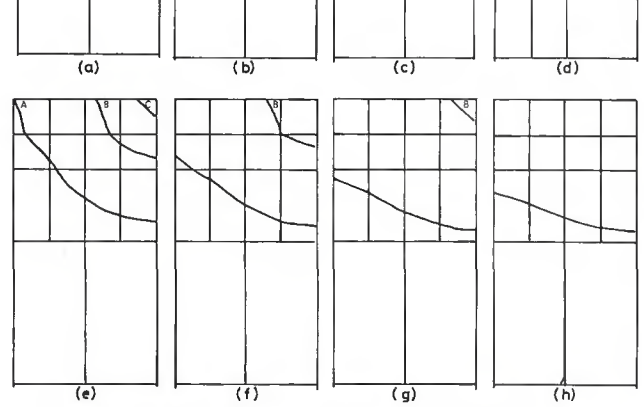

Fig. 3 — Temperature field computed using 2D cross-section analysis.

cant. Figures 4 and 5 are the cooling curves for different nodes (numbered in Fig. 1) obtained with 3D and 2D cross-sectional analysis with the hemispherical PDDF.

Figure 4 indicates that the maximum temperature developed at the node under the heat source steadily increased until the body attained maximum temperature corresponding to the heat input. Then it remained constant as long as the heat source was applied. When the heat source was removed and the body allowed to cool, the maximum temperature at the nodes began to fall. The maximum temperature attained at the starting point, which was 0.3175 cm ($^1/_8$ in.) left of plane AA, was lower than the maximum temperature attained at node 527 (on plane AA). The maximum temperature of the body stabilized after the arc traveled a distance of 0.9525 cm ($^3/_8$ in.) from the initial position. Cooling curves showed a trend similar to Gaussian distribution. Figure 5A indicates that the temperature does not follow a Gaussian shape and the fall was rather gradual. Figure 5B shows the cooling curve for node 527, which developed the maximum temperature in the 2D cross-sectional analysis.

The cooling curve for node 527 at the tip of plane AA exhibited a kink in the temperature curve around 1600°C while cooling. Other nodes did not attain this temperature; hence, the absence of the kink. During heating, the heat input continues while the body temperature increases. In 2D analysis, the highest temperature was attained at node 527, which is the tip of the plane. While cooling, in the case of 3D analysis, even though the heat source was removed, higher body temperature around plane AA helped in gradual cooling; hence, absence of the kink. However, in the case of 2D analysis, when the heat source was removed, temperature around plane AA became ambient; therefore, the cooling was faster. At approximately 1500°C, solidification took place and this resulted in a changed temperature gradient; *i.e.*, a kink.

Table 1 shows the thermal loads (reactions) computed with the 2D cross-sectional analysis using prescribed temperatures obtained from the 3D analysis. When this PDDF is used, the temperature distribution obtained with 2D analysis is the same as that obtained with 3D analysis; thus, the results of 2D analysis with modified PDDF are not included separately. Figure 6 shows the relationship between thermal load and time. It may be observed that when a hemispherical heat source was used for 2D cross-sectional analysis, the elements in general and node 527 in particular were loaded thermally only while the arc traveled through a distance of 0.79 cm ($^5/_{16}$ in.) from the initial position and were not thermally loaded thereafter. However, when the temperature from the 3D analysis was applied to the 2D analysis, the thermal loads continued beyond 0.9525 cm and the maximum temperature of the body increased to 0.9525 cm; therefore, the temperature was higher. Since the thickness is assumed infinite in the 2D cross-sectional analysis, even though the surface temperature at node 527 was higher than that obtained with 3D, the body temperature was lower. Figure 6 also illustrates that the power density does not follow a hemispherical Gaussian PDDF and the fall in temperature has a lower gradient. This double ellipsoidal PDDF produces a higher temperature in the 2D analysis than the hemispherical Gaussian PDDF.

One test that can be applied to verify the accuracy of the results of the thermal analysis is the maximum principle. It states that the maximum and minimum temperatures must be obtained on the boundary of a region, provided no sinks or source exist. Hence, the minimum temperature should not be less than 20°C, which is the initial temperature assumed for the analysis. However, it was observed that the temperature at the farthest nodes was lower than 20°C, which indicates that the mesh assumed in those regions would have to be refined to compute the temperatures more accurately. Similarly when reactions are computed, the thermal loads may be negative if the values do not converge within the prescribed number of iterations. In such cases, the number of iterations have to be increased to attain convergence and the reactions become either positive or zero. Zero reaction indicates that the node is not thermally loaded during that time step. In choosing time steps, it was found that convergence was rapid if the maximum temperature change at any node was less than 100°C in any increment. Convergence was slow and could be divergent if the maximum temperature change at any node exceeded 200°C. In particular, small time steps should be used when starting and stopping the arc. This was particularly important when the temperature moved through 600°C and the yield strength dropped sharply.

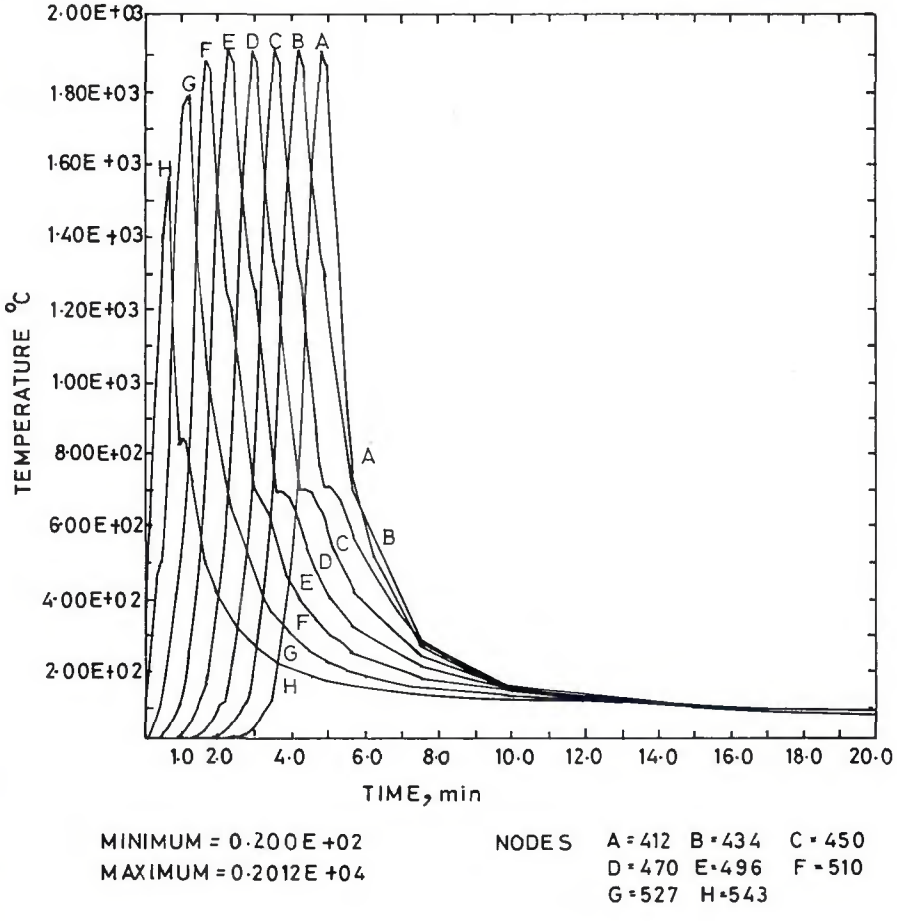

Fig. 4 — Temperature vs. time plot obtained using 3D analysis.

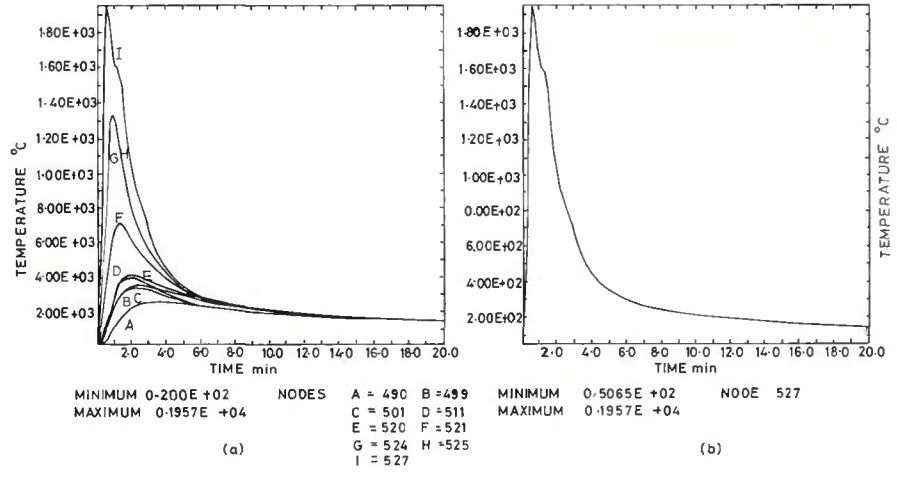

Fig. 5 — Temperature vs. time plot obtained using 2D cross-section analysis.

Conclusions

1. The analysis presented in this paper indicates that the temperature gradient in the longitudinal direction (Z-direction) is significant and should not be assumed negligible for a 2D cross-sectional analysis. However, assuming a double ellipsoidal PDDF with the appropriate parameters for the heat source in the 2D cross-sectional analysis can reduce the error.

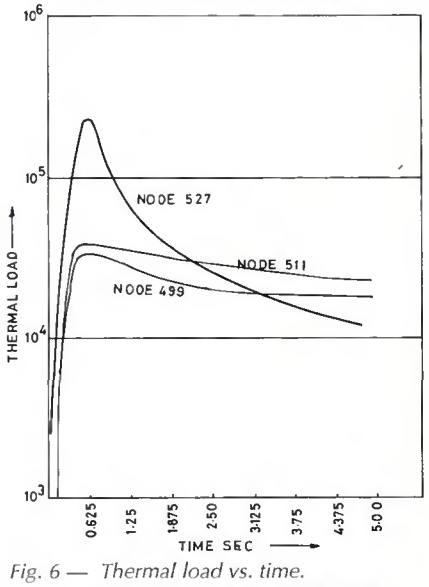

Fig. 6 — Thermal load vs. time.
FIG 6. THERMAL LOAD VS TIME

Table 1—Thermal Reactions Computed from 2-D Cross-Sectional Analysis with Prescribed Temperatures Obtained from 3-D Analysis

Node	Right Hand Side After Code	Output 1 0.104 s	Output 2 0.234 s	Output 3 0.312 s
			Reactions due to prescribed variables	
319	1	0.34433354 E−02	0.52516313 E+01	0.76409416 E+02
320	1	0.19022653 E+00	0.12708126 E−01	0.16918033 E−02
321	1	0.47750656 E+00	0.11053680 E+01	0.26195684 E+02
322	1	0.94466514 E−01	0.22739308 E+00	0.57582141 E+01
383	1	0.53703768 E+00	0.80262107 E+02	0.44768978 E+03
384	1	0.16693310 E+00	0.14763834 E+02	0.14106282 E+03
442	1	0.79797002 E+01	0.12509565 E+03	0.26934628 E+04
443	1	0.66333002 E−01	0.21242092 E+01	0.13882565 E+03
446	1	0.48611051 E+01	0.80002967 E+02	0.22644307 E+04
490	1	0.11143687 E+02	0.16476391 E+04	0.10773647 E+05
491	1	0.52315773 E−02	0.78862751 E+01	0.17494110 E+03
493	1	0.12346059 E−01	0.62618715 E+02	0.22250362 E+04
499	1	0.72218825 E+03	0.76931854 E+04	0.21313915 E+05
501	1	0.39759694 E+03	0.82471745 E+04	0.28870174 E+05
503	1	0.44637964 E−02	0.29516004 E+03	0.42452712 E+04
504	1	0.17289844 E−01	0.40280979 E−02	0.26711803 E+04
507	1	0.44757464 E−01	0.25811501 E+03	0.28084390 E+04
508	1	0.32259472 E−01	0.35610868 E+02	0.16638179 E+03
511	1	0.39766962 E+03	0.80035625 E+04	0.25611752 E+05
520	1	0.72221949 E+03	0.74939359 E+04	0.19323663 E+05
521	1	0.43487527 E+04	0.40413678 E+05	0.86323823 E+05
524	1	0.59290583 E+04	0.37953637 E+05	0.71872705 E+05
525	1	0.59290428 E+04	0.37878382 E+05	0.71512547 E+05
527	1	0.68086609 E+04	0.35151874 E+05	0.60891989 E+05

Node	Code	Output 4 0.528 s	Output 5 1.716 s	Output 6 2.808 s
			Reactions due to prescribed variables	
319	1	0.13182560 E+03	0.10439605 E+03	0.51102572 E+03
320	1	0.19751869 E+02	0.31493231 E+02	0.97842749 E+03
321	1	0.51784025 E+02	0.10217206 E+03	0.43067569 E+03
322	1	0.61218378 E+01	0.27519070 E+02	0.80525617 E+02
383	1	0.10207559 E+04	0.23081596 E+03	0.23244088 E+04
384	1	0.38998974 E+03	0.26447156 E+03	0.18920345 E+04
442	1	0.13977449 E+05	0.18320574 E+05	0.26869535 E+05
443	1	0.27302116 E+04	0.59750142 E+04	0.12041619 E+05
446	1	0.15882182 E+05	0.23677970 E+05	0.38350721 E+05
490	1	0.33952989 E+05	0.33025102 E+05	0.39712396 E+05
491	1	0.29793666 E+04	0.51958879 E+04	0.88340542 E+04
493	1	0.12183680 E+05	0.15972103 E+05	0.23401976 E+05
499	1	0.49881641 E+05	0.36469607 E+05	0.35642780 E+05
501	1	0.71807651 E+05	0.58115095 E+05	0.60711855 E+05
503	1	0.16745321 E+05	0.19037708 E+05	0.25499882 E+05
504	1	0.36450267 E+04	0.57403392 E+04	0.90835693 E+04
507	1	0.99407135 E+04	0.11064109 E+05	0.14446647 E+05
508	1	0.21468954 E+04	0.32248117 E+04	0.50281865 E+04
511	1	0.61215900 E+05	0.47864463 E+05	0.48931197 E+05
520	1	0.43845547 E+05	0.30614711 E+05	0.29064536 E+05
521	1	0.19636875 E+06	0.10770650 E+06	0.85371396 E+05
524	1	0.18698563 E+06	0.77539909 E+05	0.54277346 E+05
525	1	0.18625807 E+06	0.77122820 E+05	0.53897735 E+05
527	1	0.22894046 E+06	0.59386721 E+05	0.36123291 E+05

Node	Code	Output 7 3.43 s	Output 8 4.2 s	Output 9 4.3 s
			Reactions due to prescribed variables	
319	1	0.96824172 E−02	0.13075738 E−02	0.14071999 E−03
320	1	0.13957673 E+03	0.12625104 E+03	0.50323527 E+02
321	1	0.82753946 E−02	0.11381816 E−03	0.12394659 E−03
322	1	0.11496905 E+03	0.10068780 E+03	0.28417450 E+02
383	1	0.53912564 E+04	0.93836301 E+04	0.14257799 E+05
384	1	0.46796132 E+04	0.85653462 E+04	0.13339359 E+05
442	1	0.33455442 E+05	0.38142949 E+05	0.41532785 E+05
443	1	0.18624640 E+05	0.24938172 E+05	0.30558435 E+05
446	1	0.51599810 E+05	0.62815901 E+05	0.71948906 E+05
490	1	0.42900513 E+05	0.44023969 E+05	0.43987148 E+05
491	1	0.12061191 E+05	0.14627707 E+05	0.16502290 E+05
493	1	0.29194387 E+05	0.33367951 E+05	0.36129457 E+05
499	1	0.33531118 E+05	0.30678829 E+05	0.28079035 E+05
501	1	0.59234364 E+05	0.55954683 E+05	0.52437585 E+05
503	1	0.29591693 E+05	0.31935094 E+05	0.32990988 E+05
504	1	0.11756776 E+05	0.13658152 E+05	0.14836948 E+05

507	1	0.16402441 E+05	0.17419404 E+05	0.17769065 E+05
508	1	0.64265902 E+04	0.73865228 E+04	0.79486226 E+04
511	1	0.47344671 E+05	0.44529350 E+05	0.41641998 E+05
520	1	0.27129336 E+05	0.24746014 E+05	0.22679605 E+05
521	1	0.71196743 E+05	0.59800326 E+05	0.51263391 E+05
524	1	0.42071425 E+05	0.34018247 E+05	0.28213691 E+05
525	1	0.41727978 E+05	0.33630444 E+05	0.27785998 E+05
527	1	0.25449054 E+05	0.19239793 E+05	0.15384738 E+05
		Output 10 5 s	Output 11 10 s	Output 12 15 s
Node	Code		Reactions due to prescribed variables	
319	1	0.12016532 E−02	0.33264873 E−03	0.11539763 E−03
320	1	0.77841749 E−02	0.46653119 E−01	0.13628797 E+02
321	1	0.10600552 E−04	0.29480070 E−03	0.10348706 E−03
322	1	0.92990772 E−02	0.90993063 E−01	0.11873560 E+02
383	1	0.19657079 E+05	0.43473489 E+04	0.51991648 E+03
384	1	0.18634581 E+05	0.40940987 E+04	0.45897820 E+03
442	1	0.43981042 E+05	0.10754064 E+05	0.24473193 E+04
443	1	0.35289728 E+05	0.83323195 E+04	0.15929675 E+04
446	1	0.79191787 E+05	0.19058869 E+05	0.40256396 E+04
490	1	0.43436323 E+05	0.10936389 E+05	0.28114059 E+04
491	1	0.17762777 E+05	0.43129142 E+04	0.95044844 E+03
493	1	0.37807896 E+05	0.92873866 E+04	0.21572592 E+04
499	1	0.25945840 E+05	0.67265159 E+04	0.19216850 E+04
501	1	0.49338280 E+05	0.12689410 E+05	0.35271919 E+04
503	1	0.33219957 E+05	0.83122802 E+04	0.20853611 E+04
504	1	0.15453603 E+05	0.38122388 E+04	0.90189765 E+03
507	1	0.17712271 E+05	0.44511067 E+04	0.11358156 E+04
508	1	0.82120307 E+04	0.20325803 E+04	0.48771775 E+03
511	1	0.39094072 E+05	0.10084021 E+05	0.28315080 E+04
520	1	0.20987153 E+05	0.54479810 E+04	0.15631881 E+04
521	1	0.45382354 E+05	0.12021885 E+05	0.36817675 E+04
524	1	0.24525404 E+05	0.65535461 E+04	0.20605817 E+04
525	1	0.24055768 E+05	0.64386493 E+04	0.20343695 E+04
527	1	0.13032406 E+06	0.35195628 E+04	0.11413519 E+04

Maximum Temperature change at any node is less than 2 deg.

2. For any physically attainable temperature field, a PDDF exists that would create that field with either the 2D cross-sectional or the 3D analysis.

3. For a 2D cross-sectional analysis, the real PDDF can be modified to yield the correct 3D temperature field at a particular instant of time.

4. The modified PDDF can be evaluated by prescribing the correct 3D temperature field to the 2D cross-sectional problem. The resulting reactions are the PDDF.

5. For the case in which the hemispherical PDDF is correct, the modified PDDF for the 2D cross-sectional analysis is shown to be very close to the double ellipsoidal PDDF proposed in Ref. 4. To correct for the lack of longitudinal heat flow in the 2D model, the modified PDDF rises more quickly and falls more slowly than the hemispherical PDDF.

Acknowledgments

V. Kamala acknowledges the kind permission accorded him by BHEL, Corporate Research and Development Division, Hyderabad, India to pursue postdoctoral research at the Center for Advanced Studies in Computer Aided Design and Engineering (CASCADE), Carleton University, Ottawa. The financial support of ASERC A2 922 (J. Goldak), NSERC Strategic Grant GI529 (J. Goldak) and AMCA International are appreciated.

References

1. Rosenthal, D. *The theory of moving sources of heat and its application to metal treatments,* Trans. ASME, Vol. 68, 1946, pp. 849–865.

2. Myers, P. S., Uyehara, O. A. and Borman, G. L. *Fundamentals of heat flow in welding,* Welding Research Council bulletin, No. 123, New York, 1967.

3. Goldak, J. A., Patel, B., Bibby, M. and Moore, J. E. *Computational weld mechanics,* AGARD Structures and Materials 61st Panel Meeting, Oberammergau, Germany, Sept. 8–13, 1985.

4. Goldak, J. A., Bibby, M., Moore, J. E., House, R. and Patel, B. *Computer modeling of heat flow in welds,* Met. Trans. B, Vol. 17B, Sept. 1986, pp. 587–600.

5. Paley, Z. and Hibbert, P. D. Compution of temperatures in actual weld designs, *Welding Journal* 54(11): 385-s to-392-s

6. Westby, O. *Temperature distribution in the workpiece by welding,* Department of Metallurgy and Metal Working, The Technical University, Trondheim, Norway, 1968.

7. Eager, T. W. and Tsai, N. S. Temperature fields produced by travelling distributed heat sources, *Welding Journal* 62(12): 346-s to 355-s.

8. Krutz, G. W. and Segerlind, L. J. Finite Element Analysis of welded structures, *Welding Journal 57(7):* 211-s to 216-s.

9. Pavelic, V., Tanbakuch, O. A., Uyehara, O. A. and Myers, P. S. Experimental and computed temperature histories in Gas Tungsten Arc welding thin plates, *Welding Journal* 48(7): 295-s to 305-s.

10. Friedman, E. *Thermomechanical analysis of the welding process using the Finite Element method,* J. of Pressure Vessel Technology, Trans. ASME, Vol.97, 1975, pp. 206–213.

11. Raichur, X. S. *Thermal analysis on personal Computers using Finite Elements,* Conf. Proc., Computer Aided Engineering Application, ASME PUP, Vol.126, 1987, pp. 65–71.

12. Goldak, J. A., Chakravarti, A. P. and Bibby, M. *A new Finite Element model for welding heat sources,* Metallurgical Transactions, Vol.15B, 1984, pp. 299–305.

13. McDill, M., Goldak, J. A., Oddy, A. and Bibby, M. J, *Iso-parametric quadrilaterals and Hexahedrons for Mesh Grading algorithms,* Communications in Applied Numerical Methods.

14. The British Iron and Steel Association. *Physical constants of some commercial steels at elevated temperatures,* London, Butterworths Scientific Publications, 1953.